nature physics

SUPPLEMENTARY INFORMATION

DOI: 10.1038/NPHYS4117

In the format provided by the authors and unedited.

Topological triplon modes and bound states in a Shastry–Sutherland magnet

P. A. McClarty,[1,2] F. Krüger,[1,3] T. Guidi,[1] S. F. Parker,[1] K. Refson,[1,4] A. W. Parker,[5] D. Prabhakaran,[6] and R. Coldea[6]

[1] *ISIS, Science and Technology Facilities Council, Rutherford Appleton Laboratory, Didcot OX11 0QX, United Kingdom.*

[2] *Max Planck Institute for the Physics of Complex Systems, Nöthnitzer Strasse 38, 01187 Dresden, Germany.*

[3] *London Centre for Nanotechnology, University College London, Gordon Street, London, WC1H 0AH, United Kingdom.*

[4] *Department of Physics, Royal Holloway, University of London, Egham TW20 0EX, United Kingdom.*

[5] *Central Laser Facility, Science and Technology Facilities Council, Rutherford Appleton Laboratory, Didcot OX11 0QX, United Kingdom.*

[6] *Clarendon Laboratory, University of Oxford, Parks Road, Oxford OX1 3PU, United Kingdom.*

(Dated: March 27, 2017)

I. ANOMALOUS TERMS

Anomalous quadratic terms $t^\dagger_{A\alpha}t^\dagger_{B\beta}$ and $t_{A\alpha}t_{B\beta}$ arise from the bond-operator representation of the coupling between spins of neighboring dimers and are proportional to D' and DJ'/J, exactly as the triplon hopping terms. Including these terms, the quadratic triplon Hamiltonian can be written as

$$\tilde{H}_{\rm ST} = \frac{1}{2}\int_{\boldsymbol{k}} \left(T^\dagger_{\boldsymbol{k}}, T_{-\boldsymbol{k}}\right) \begin{pmatrix} \Lambda_{\boldsymbol{k}} & \Pi_{\boldsymbol{k}} \\ \Pi^\dagger_{\boldsymbol{k}} & \Lambda^t_{-\boldsymbol{k}} \end{pmatrix} \begin{pmatrix} T_{\boldsymbol{k}} \\ T^\dagger_{-\boldsymbol{k}} \end{pmatrix},$$

where the six-dimensional triplon operators $T_{\boldsymbol{k}}$ and coupling matrices $\Lambda_{\boldsymbol{k}}$ have been defined in the Methods section. The coupling matrix for the anomalous terms is given by

$$\Pi_{\boldsymbol{k}} = \begin{pmatrix} 0 & C_{\boldsymbol{k}} \\ C^\dagger_{\boldsymbol{k}} & 0 \end{pmatrix},$$

and is identical to the triplon hopping matrix between neighboring dimers. It has been argued by Romhanyi *et al.*[1] that the anomalous terms have a negligible effect since they do not change the triplon energies to linear order (they renormalize the single-triplon parameters to second order in perturbation theory). In order to investigate this further, we compare the triplon excitation spectra in the presence and absence of the anomalous terms. It is straightforward to diagonalize the quadratic triplon Hamiltonian $\tilde{H}_{\rm ST}$ by a Bogoliubov transformation. This includes the anomalous terms to infinite order. In Fig. 1 the triplon excitation spectra are shown in zero field and for the parameters of Ref. [1]. The corrections due to the anomalous terms are indeed very small and affect only the upper and lower triplon bands away from the M point.

Treating the anomalous terms in second order perturbation theory it is possible to work out the leading terms that renormalize the triplon dispersion. We obtain triplon hopping terms $\sim \frac{(D'_\perp)^2}{J}(t^\dagger_{ix}t_{jx} + t^\dagger_{iy}t_{jy} + \text{h.c.})$ and $\sim \frac{(D'_{\parallel,\rm eff})^2}{J}(t^\dagger_{ix}t_{jy} + t^\dagger_{iy}t_{jx} + \text{h.c.})$ between NNN dimers, which are on the same sub-lattice. Note that we have already included an isotropic NNN hopping term $J_{\rm FN}$ in the single-triplon Hamiltonian. Similar hopping terms are also generated between 3rd nearest neighbor dimers. Relative to the triplon bandwidth $W \sim D'$ we therefore expect corrections of the order of $D'/J \simeq 3\%$.

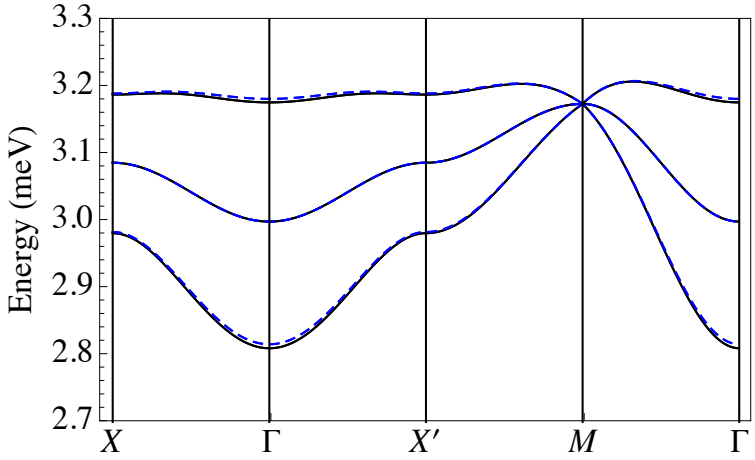

FIG. 1. **Effect of the anomalous terms.** Comparison of the triplon excitation spectra with (dashed lines) and without (solid lines) the anomalous terms, using the model of Ref. [1] in zero field.

II. SINGLET BOUND STATE

To third order in perturbation theory in J'/J there are two closed sectors of four two-triplon states. These states are illustrated in Fig. 2.

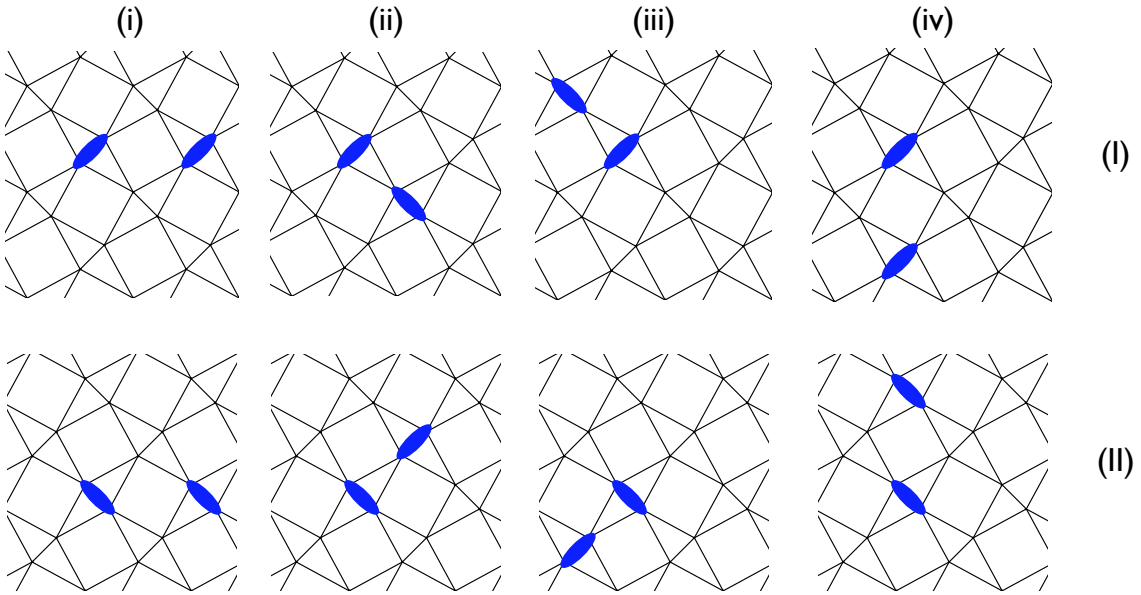

FIG. 2. **Basis states of two triplon bound states.** States are divided into two sectors (I and II) which form different blocks in the Hamiltonian and each sector contains four states (i)-(iv).

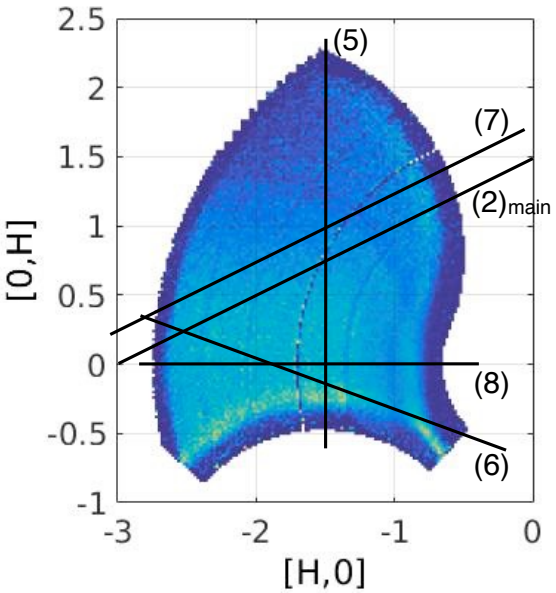

FIG. 3. **Lines in reciprocal space** The plot shows the available data at 3 meV. Lines in $\boldsymbol{Q}$ are marked along which dispersion picks were taken for the fitting procedure. Plots of the data are shown along these paths in the main text and the remainder of the supplementary section. Labels refer to the figure numbers where data is shown.

III. FURTHER COMPARISON BETWEEN THEORY AND EXPERIMENT

Here we present a sequence of figures showing the experimental inelastic neutron scattering intensity together with the calculated inelastic neutron cross section. Figs. 5- 9 are energy-momentum cuts at 0, 0.7 T, 1.4 T and 2.8 T with the intensity represented through gradations in colour. These are compared with the best fits obtained from our full model (shown in the lower set of panels in each figure). The remaining figures 10- 11 are energy cuts at constant momentum, showing more clearly a quantitative comparison between the calculated and measured intensities. The cuts were produced using HORACE with the theoretical cuts being extracted from the tabulated cross section using the same momentum binning as the corresponding experimental cuts. The width of the calculated peaks was set equal to the calculated energy resolution $\sim 70\mu$eV at 3 meV energy transfer, leaving only the overall intensity scale as a free parameter which is set by a single peak at $[-2, 0]$.

The comparisons illustrate that both dispersions and intensities are captured by the model. In addition to the $[-1 + H, 1 + H]$ cut in the main text (also Fig. 4), we show here

$[H, 0]$ (Fig. 5), $[-0.5 - H, -0.5 + H]$ (Fig. 6), $[-1.2 + H, -1.2 + H]$ (Fig. 7) and $[-1.5, H]$ (Fig. 8). The field independence of the additional mode, which we have identified as an $S = 0$ bound state of two triplons, is most clearly visible in Fig. 4. At energies $3.25 - 3.35$ meV, slightly above the triplon bands, we find rings of intensity in the $[H, K]$ momentum plane (Fig. 9) that meet the Brillouin zone edge at about 3.8 meV. Note that slightly above the triplon bands, the bound state is visible because of the relatively strong admixture of single-triplon character. The theoretical model reproduces the inhomogeneous intensity distribution over the rings.

Figs. 10 and 11 show six energy cuts at different points in momentum space. These are chosen to be representative of the fit across the entire four dimensional volume of measured intensity. We emphasise that the intensities were not directly constrained by the fit which was carried out using the dispersions alone. Nevertheless, the calculated intensities from this fit are in satisfactory quantitative agreement with the measured intensities. Note that because of the small energy gaps between bands, not all bands are resolved, even at 2.8 T. This quasi degeneracy results in a broader, unresolved peak at the centre.

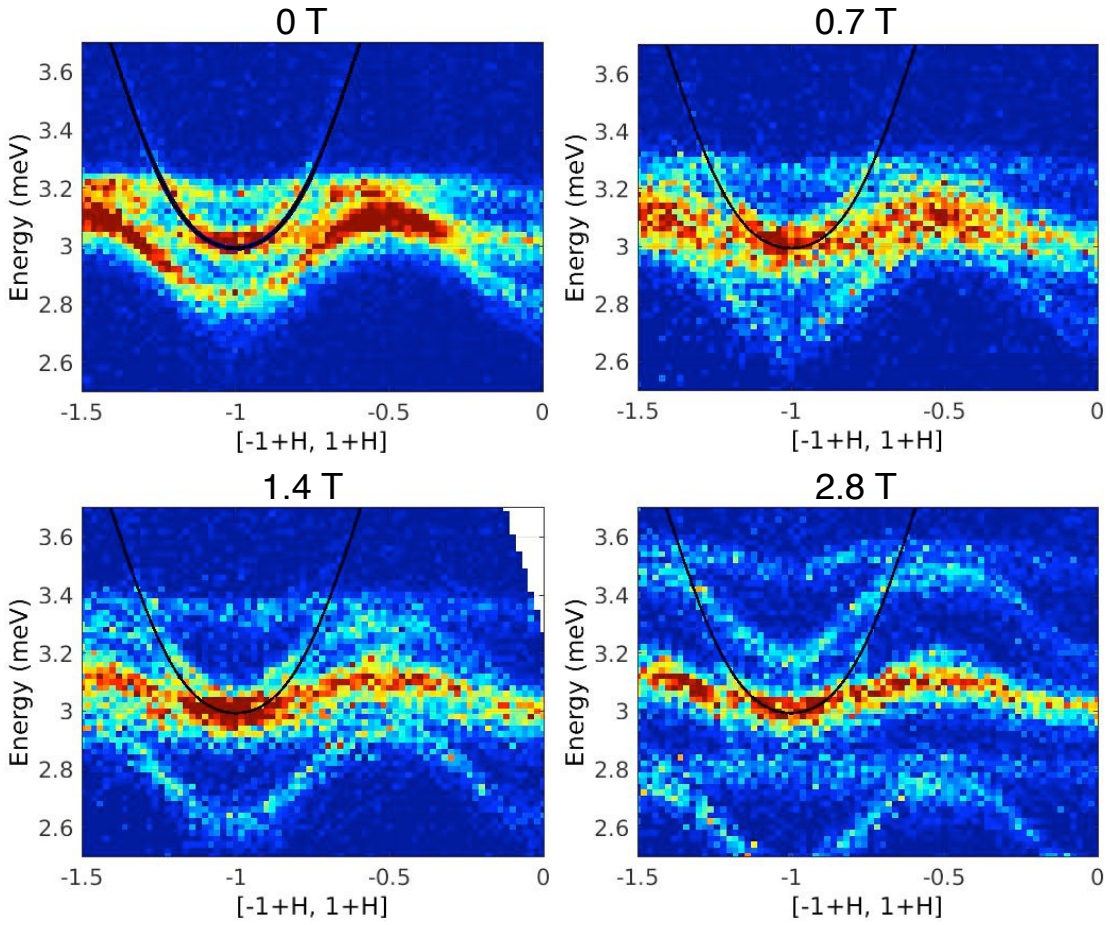

FIG. 4. **Field independence of singlet mode** Panels showing cuts along $[-1+H, 1+H]$ in four different fields - in reading order 0T, 0.7T, 1.4T and 2.8T. A polynomial fit to the dispersive mode intersecting the singlet triplon excitations is identically plotted on top of these panels to illustrate the field independence of this mode.

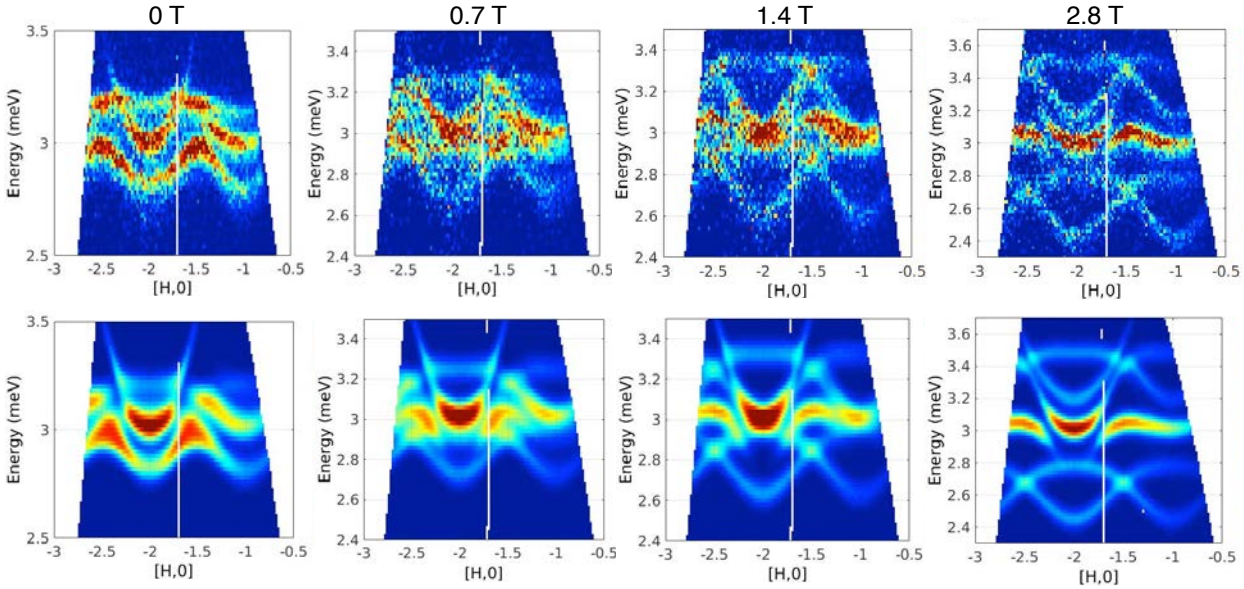

FIG. 5. **Experimental cuts along $[H, 0]$ and corresponding dynamical structure factor of the model described in the main text. The intensity scale is the same as in Fig. 2 (main text).**

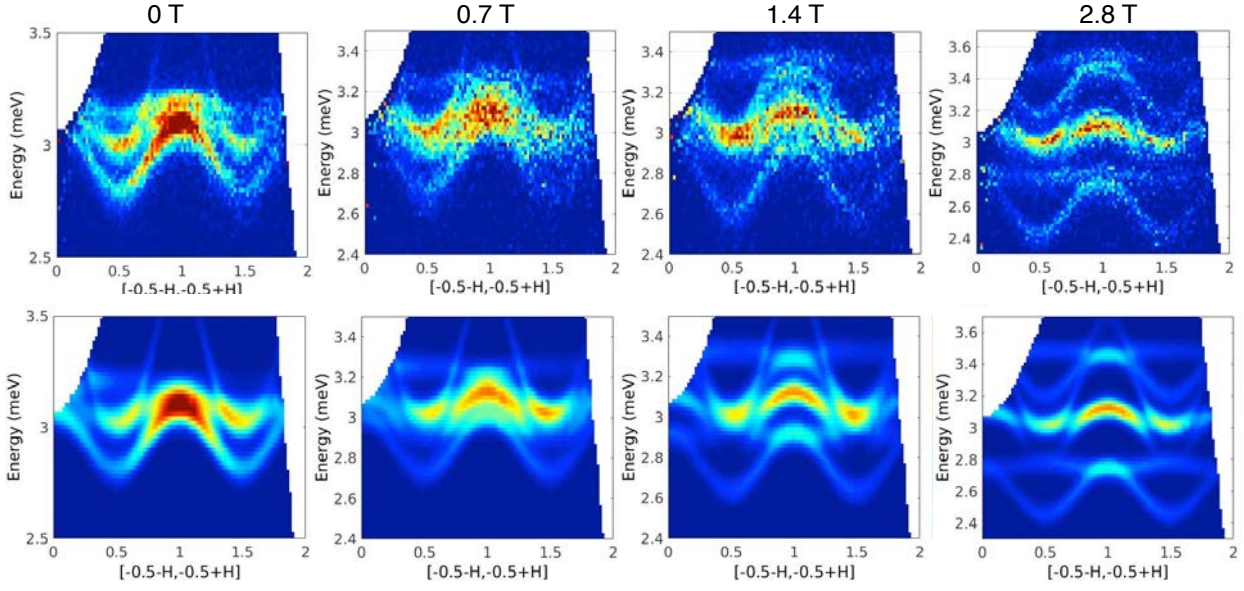

FIG. 6. **Experimental cuts along $[-0.5 - H, -0.5 + H]$ and corresponding dynamical structure factor of the model described in the main text. The intensity scale is the same as in Fig. 2 (main text).**

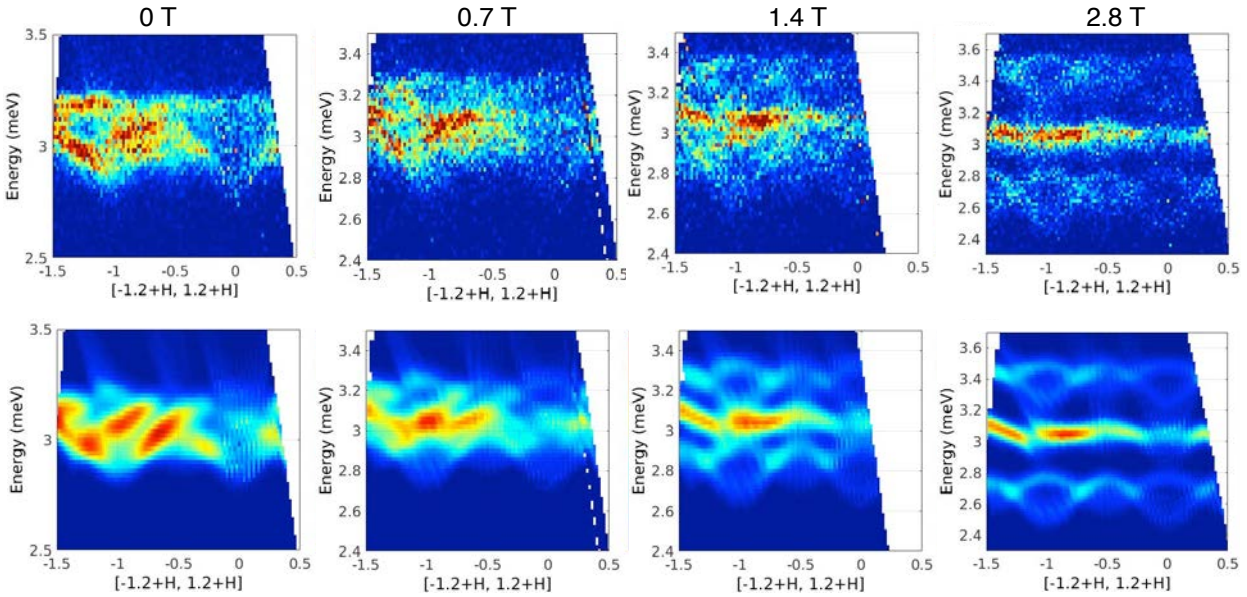

FIG. 7. **Experimental cuts along $[-1.2 + H, -1.2 + H]$ and corresponding dynamical structure factor of the model described in the main text. The intensity scale is the same as in Fig. 2 (main text).**

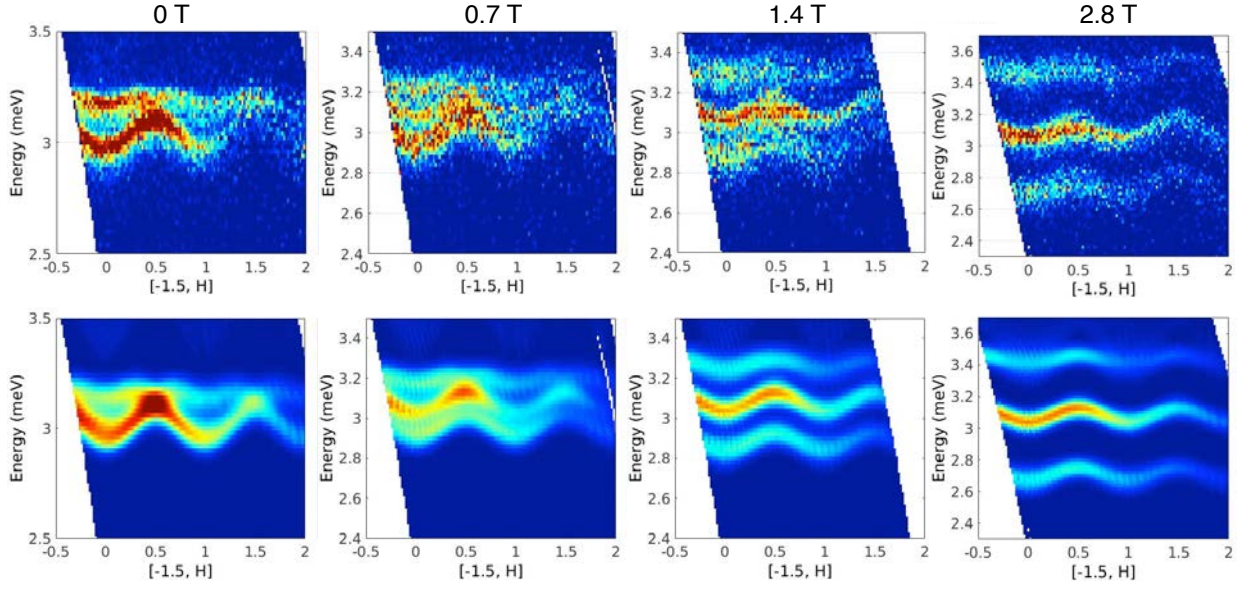

FIG. 8. **Experimental cuts along $[-1.5, H]$ and corresponding dynamical structure factor of the model described in the main text. The intensity scale is the same as in Fig. 2 (main text).**

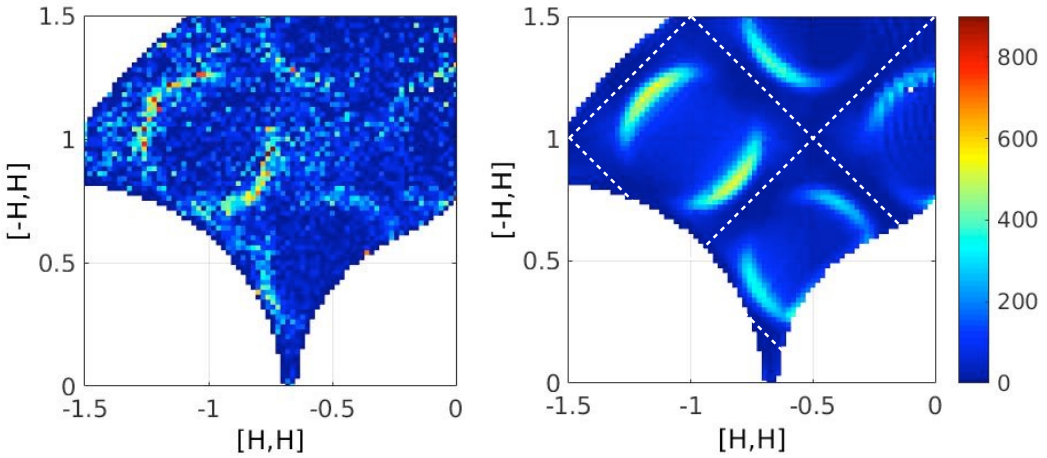

FIG. 9. **Bound-state mode at constant energy slightly above the triplon bands.** (a) A constant energy cut showing rings of intensity in the $[HH]/[-HH]$ plane integrated over the range $3.25-3.35$ meV and over the measured $[00L]$ direction at zero field. (b) The calculated dynamical structure factor for comparison with the experiment. The singlet bound state becomes visible in the dynamical structure factor because of the hybridization with the triplon excitations and the admixture of single-triplon weight. The Brillouin zone boundaries are indicated by dashed lines.

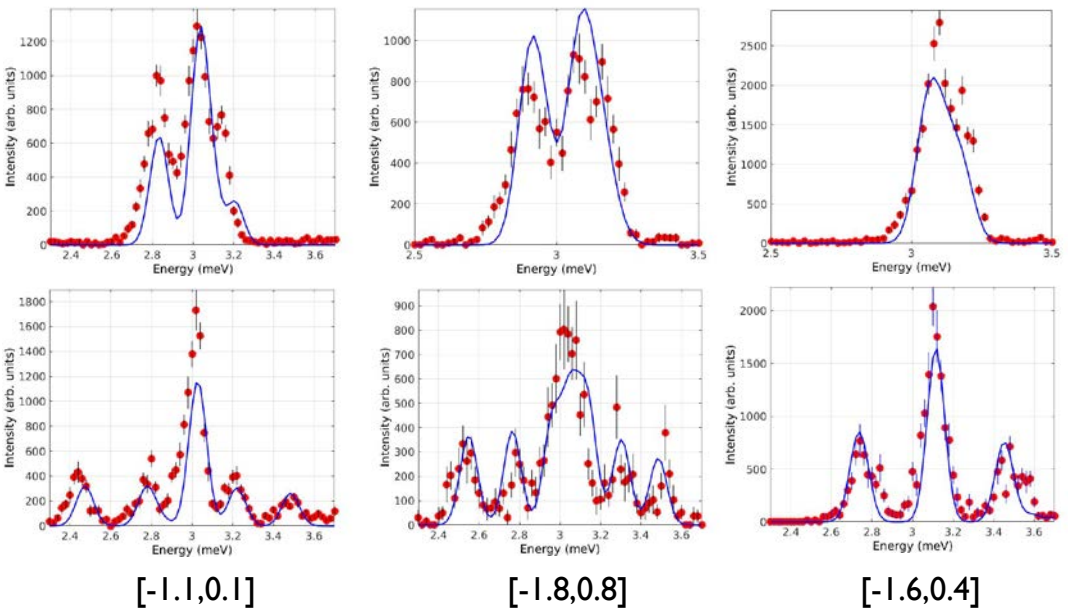

FIG. 10. **Selection of constant Q cuts.** The upper panel is zero field data and the lower panel data at 2.8 T. Red points are the measured intensties and the solid line is the calculated intensity.

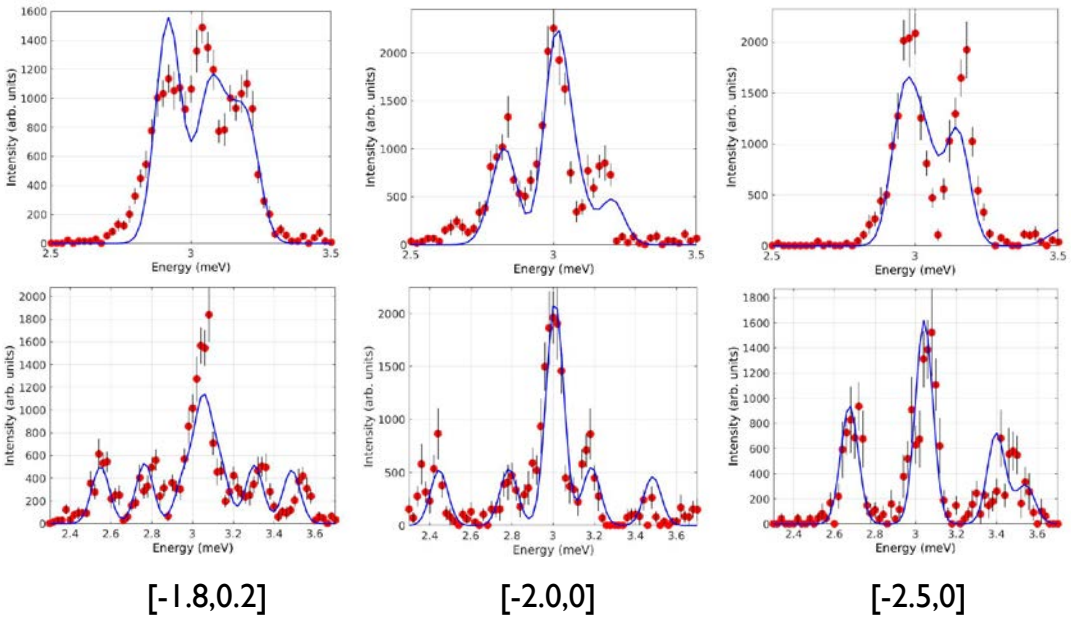

FIG. 11. **Further constant Q cuts.** The upper panel is zero field data and the lower panel data at 2.8 T. Red points are the measured intensties and the solid line is the calculated intensity.

IV. DISCUSSION OF PHONON SCENARIO

The identification of the additional mode in the spectrum with an $S = 0$ bound state provides a consistent and well-motivated explanation for the experimental data. However, we now consider the possibility that this mode is, instead, a phonon mode. It is unlikely to be an acoustic mode because no intensity is present below the lowest single triplon band and the latter mode shows no hybridization gap. This leaves the possibility that the mode is an optical phonon. One would expect a phonon mode to be present even when the magnetic form factor suppresses the magnetic intensity or when the temperature washes out the triplon signal. However, the intensity of the mode over the range of $|\boldsymbol{Q}|$ measured in our experiment is nontrivial and suggestive of being present only through the coupling to the triplon modes. Indeed, at 15 K when the triplon intensity is absent, the additional mode is also not present. It is therefore likely that the mode is visible in our experiment only because it is either entirely magnetic or because of a magnetoelastic coupling. A consideration of the magnetoelastic coupling suggests that it would take the form of a coupling to a triplon density whereas the mode appears to hybridize linearly with the triplons. This is accounted for naturally in the bound state scenario. Finally, we turn to observations of low energy phonons coming from other experiments. Previous neutron scattering experiments[2] have only been able to resolve optical phonon modes at energies above 15 meV while Raman spectra have been interpreted as showing only magnetic modes below about 7 meV.[3,4] While these considerations suggest that the new mode is entirely magnetic and not structural further experiments are desirable to rigorously rule out a phonon scenario.

V. THERMAL HALL EFFECT

The Chern number is connected to observable quantities. In integer quantum Hall systems, for example, the Chern number is related to the quantized Hall conductance.[5] A bosonic analogue of this result for the case when the band is thermally populated is the thermal Hall effect which, rather than depending on the Chern number and yielding a quantized response instead depends on the magnitude of the Berry curvature in thermally occupied parts of the band.

We assume that the transverse thermal conductivity comes from the response of triplons

to the Berry curvature in the triplon bands as given by

$$\kappa_{\alpha\beta} = -\frac{k_B^2 T}{\hbar L} \sum_{\mathbf{k},n} c_2[\rho(\omega_{n,\mathbf{k}})] F_{\alpha\beta}^{(n)}(\mathbf{k}) \quad (1)$$

where $F_{\alpha\beta}^{(n)}(\mathbf{k})$ is the Berry curvature in the nth band and

$$c_2(\rho) \equiv (1+\rho)\left(\log\frac{1+\rho}{\rho}\right)^2 - (\log\rho)^2 - 2\mathrm{Li}_2(-\rho).$$

Here $\rho = (\exp(\beta\omega) - 1)^{-1}$ is the Bose distribution function and Li is the polylog function. $L = 3.32$Å is the layer thickness. The formula above was derived for magnons by Matsumoto and Murakami[6] building on work by Katsura, Nagaosa and Lee.[7] In the latter work, the magnon rotational motion was omitted leading to a formula that depends only on the Berry curvature in the low temperature limit. The formula is directly applicable to the triplon problem. Fig. 12 shows the thermal Hall conductivity κ_{xy} over a range of magnetic fields at 5 K and 7.5 K in $SrCu_2(BO_3)_2$ including only the single triplon sector. The maximum at around 0.7 T is due to the maximum in the low energy density of triplon states at this field owing to the fact that the touching point see-saws from the Brillouin zone corner at 0 T to the zone centre at 1.4 T with the average energy anchored by the $S = 0$ triplon. The topological transition is visible as a kink in the Hall effect resulting from a spike in the Berry curvature at the touching point in the Brillouin zone.

The result of the Hall effect calculation in the presence of our model including the singlet bound state using parameters obtained by fitting the INS data is shown in Fig. 12(b). While the Hall effect again exhibits a broad maximum as the field is increased, the detailed variation is quite different from the case with only single triplons. This is largely due to the fact that the hybridization with the bound state increases the number of topological transitions as a function of field.

To appreciate this we calculated the Chern numbers of the bands in a very small transverse field that gaps out the Brillouin zone corners so that the Chern number calculation is straightforwardly well-defined. The main text has a figure showing the Chern numbers of the low energy bands at four fields. These figure demonstrates that the possible Chern numbers and number of topologically nontrivial bands is increased relative to the single triplon case. In addition, nontrivial bands persist well above the 1.4 T upper critical field of the single triplon case. The kinks in the thermal Hall effect correlate with topological transitions between pairs of bands with the effect being greatest at about 0.6 T and again at 2.6

T where the Chern number of the lowest-lying nontrivial band changes. Further transitions in higher bands occur at a succession of fields between 0 T and 3 T.

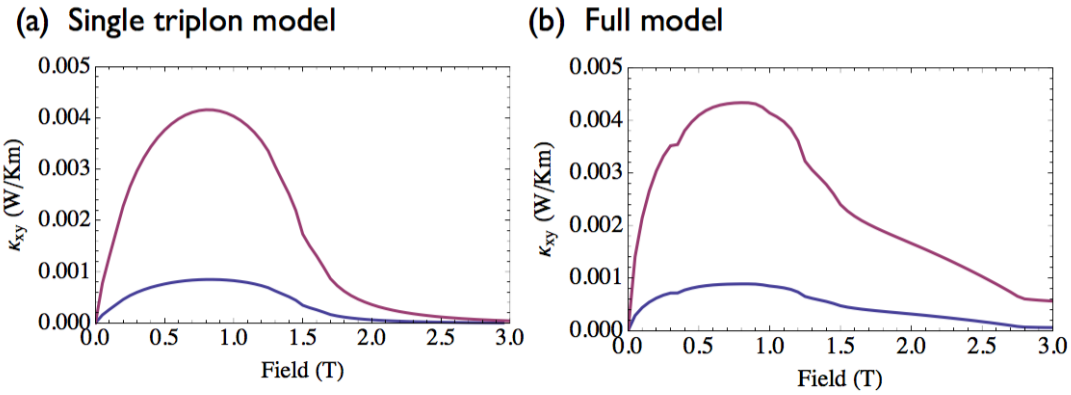

FIG. 12. **Calculated thermal Hall conductivity in $SrCu_2(BO_3)_2$.** Plot of κ_{xy} as a function of the magnetic field applied along the c direction at 5 K (blue) and 7.5 K (red).

It is evident from Fig. 12 that the thermal Hall effect does not imply the existence of Chern bands. The robust observable consequence of Chern bands is the presence of chiral edge states as we now discuss.

VI. FIELD DEPENDENCE OF THE EDGE STATES

From the Chern number calculation we have seen that because of the anisotropy and the hybridization with the bound state, the magnetic excitation spectra contain various bands with non-trivial topology. As a function of field there exist various topological transitions involving different pairs of bands. This is also reflected by the rich structure of the thermal Hall effect. In Fig. 13 we present the complex field dependence of the edge states that are present on a strip of 20 rows of dimers.

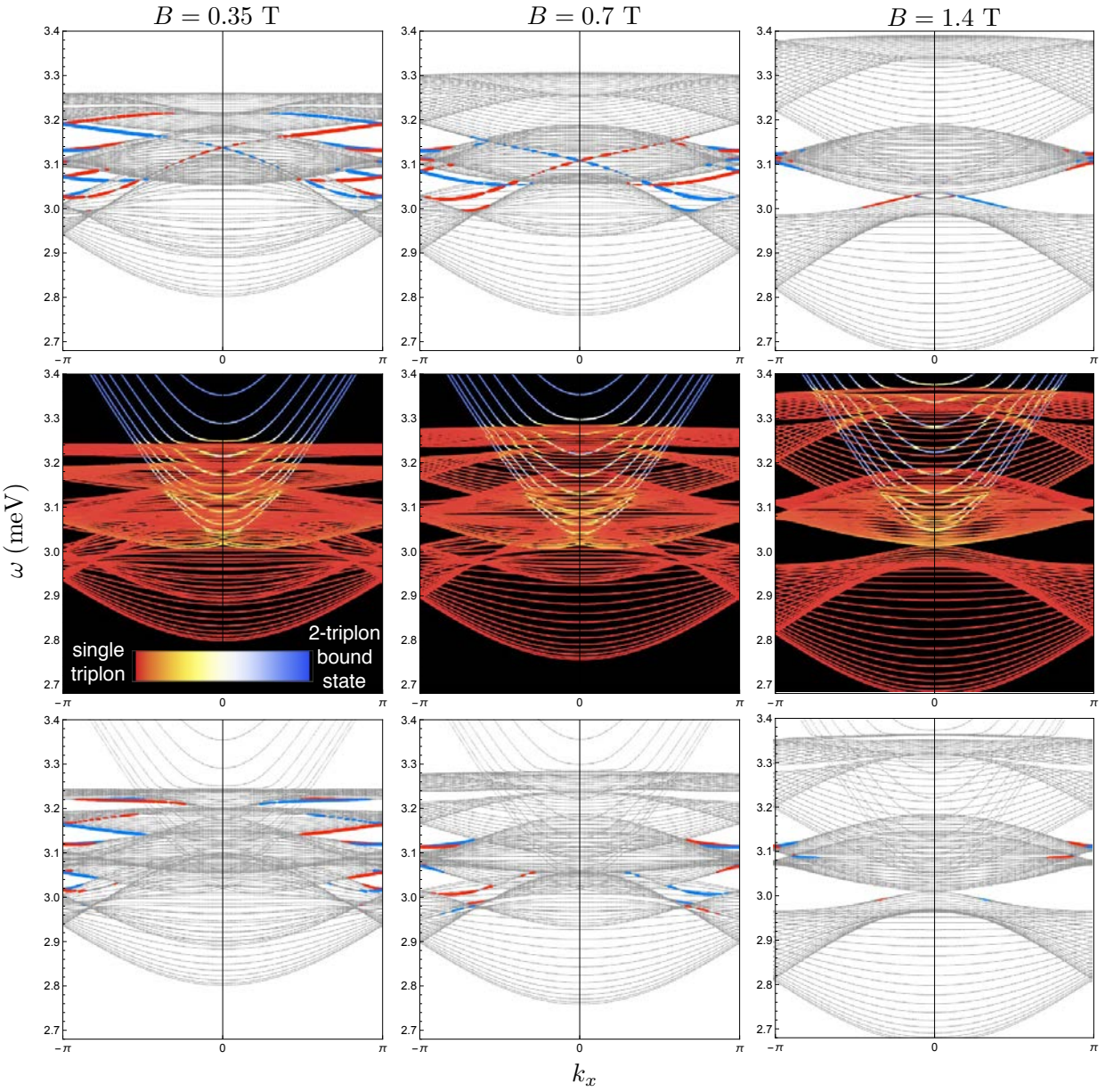

FIG. 13. **Excitation spectra and edge states of a sample with a strip geometry for different values of the magnetic field.** The top row shows the spectra for our model without the bound state. Modes that are localized near the top and bottom of the strip are colored in blue and red, respectively. The middle row shows the hybridization between the triplon excitations and the singlet bound state. The edge states are highlighted in the bottom row.

[1] J. Romhanyi, K. Penc, and R. Ganesh, Hall effect of triplons in a dimerized quantum magnet, Nature Comm. **6**, 6805 (2015).

[2] S. Haravifard, B. D. Gaulin, Z. Yamani, S. R. Dunsiger, and H. A. Dabkowska, Neutron scattering from the static and dynamic lattice of $SrCu_2(BO_3)_2$ in its Shastry-Sutherland singlet ground state, Phys. Rev. B **85**, 134104 (2012).

[3] P. Lemmens *et al.*, Collective Singlet Excitations and Evolution of Raman Spectral Weights in the 2D Spin Dimer Compound $SrCu_2(BO_3)_2$, Phys. Rev. Lett. **85**, 2605 (2000).

[4] A. Gozar, B. S. Dennis, H. Kageyama and G. Blumberg, Symmetry and light coupling to phononic and collective magnetic excitations in $SrCu_2(BO_3)_2$, Phys. Rev. B **72** 064405 (2005).

[5] D. J. Thouless, M. Kohmoto, M. P. Nightingale, and M. den Nijs, Quantized Hall Conductance in a Two-Dimensional Periodic Potential, Phys. Rev. Lett. **49**, 405 (1982).

[6] R. Matsumoto and S. Murakami, Theoretical Prediction of a Rotating Magnon Wave Packet in Ferromagnets, Phys. Rev. Lett. **106** 197202 (2011).

[7] H. Katsura, N. Nagaosa, and P. A. Lee, Theory of the thermal Hall effect in quantum magnets, Phys. Rev. Lett. **104**, 066403 (2010).